Characterization of precipitates in an Al-Zn-Mg alloy processed by ECAP and subsequent annealing

Mohamed A. Afifi, Ying Chun Wang, Pedro Henrique R. Pereira, Yangwei Wang, Shukui Li, Yi Huang, Terence G. Langdon

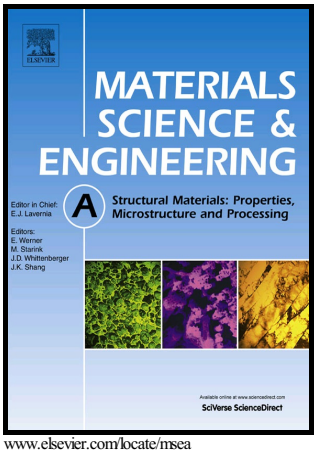

www.elsevier.com/locate/msea

PII: S0921-5093(17)31553-8
DOI: https://doi.org/10.1016/j.msea.2017.11.091
Reference: MSA35806

To appear in: *Materials Science & Engineering A*

Received date: 5 September 2017
Revised date: 5 November 2017
Accepted date: 22 November 2017

Cite this article as: Mohamed A. Afifi, Ying Chun Wang, Pedro Henrique R. Pereira, Yangwei Wang, Shukui Li, Yi Huang and Terence G. Langdon, Characterization of precipitates in an Al-Zn-Mg alloy processed by ECAP and subsequent annealing, *Materials Science & Engineering A*, https://doi.org/10.1016/j.msea.2017.11.091

Characterization of precipitates in an Al-Zn-Mg alloy processed by ECAP and subsequent annealing

Mohamed A. Afifi[a], Ying Chun Wang[a,b], Pedro Henrique R. Pereira[c], Yangwei Wang[a,b], Shukui Li[a,b], Yi Huang[c], Terence G. Langdon[c]

[a] School of Materials Science and Engineering, Beijing Institute of Technology, Beijing 100081, China
[b] National Key Laboratory of Science and Technology on Materials under Shock and Impact, Beijing 100081, China
[c] Materials Research Group, Faculty of Engineering and the Environment, University of Southampton, Southampton SO17 1BJ, UK

Abstract

Experiments were conducted to examine the influence of equal-channel angular pressing (ECAP) and post-ECAP annealing on the microstructures of an Al-Zn-Mg alloy. The results show that precipitates, mainly of the η', η ($MgZn_2$), T ($Al_{20}Cu_2Mn_3$) and E ($Al_{18}Mg_3Cr_2$) phases, are fragmented to fine spherical precipitates during ECAP processing for 4 and 8 passes. After post-ECAP annealing at 393 and 473 K for 20 h, precipitates with larger sizes lie primarily along the grain boundaries and finer particles are evenly distributed within the grains. Increasing the numbers of ECAP passes from 4 to 8 leads to an increase in the volume fraction of the finer precipitates in the ECAP-processed and annealed alloy. After 4 passes and heat treatment at 473 K, the precipitates are slightly larger compared with the alloy processed under identical conditions and annealed at 393 K. Nevertheless, significant coarsening is evident after processing for 8 passes and increasing the annealing temperature from 393 to 473 K. Different types of precipitates are effective in impeding grain growth during the post-ECAP annealing even at 473 K for 20 h. In addition, η precipitates form within the T and E phases after both ECAP and post-ECAP annealing.

Keywords: Al-Zn-Mg alloy; Equal-channel angular pressing (ECAP); Grain stability; Heat treatment; Precipitates.
Corresponding author: Ying Chun Wang, e-mail: wangyc@bit.edu.cn

1. Introduction

High strength 7xxx series (Al–Zn–Mg) alloys are widely used in the aerospace and automobile industries as structural materials [1,2]. Processing by severe plastic deformation (SPD) as in equal-channel angular pressing (ECAP) [3-6] is recognized as an effective strategy to enhance the mechanical properties of Al alloys by producing ultrafine-grained (UFG) microstructures with high densities of dislocations. These dislocations are reorganized during the multiple passes of ECAP to form fine subgrains or ultrafine grains [6,7]. In addition, second phase particles may develop in Al alloys during SPD processing [8,9]. These particles consist primarily of fine precipitates and dispersoid phases in Al-Zn-Mg alloys [10]. During aging treatment, the precipitation process follows a fixed transformation sequence, given by coherent GP zones→semi-coherent η'→incoherent η, which is controlled by the precipitation kinetics and thermodynamics [11]. Dispersoids are intermetallic particles formed usually from elements such as Cr, Mn and Zr that have low solubility in Al alloys at all temperatures, as with Al_3Zr precipitates [11]. Rod-like η precipitates can be broken into small spherical particles during ECAP processing and these are thermally stable and very effective in restraining grain growth during heating [12-14]. Accordingly, the presence of fine precipitates and dispersoids significantly improves the thermal stability of deformed microstructures [15-21].

Several reports are now available describing the evolution of precipitates and dispersoids in Al alloys during SPD processing and subsequent heat treatments, and these data provide information on their underlying properties [8,9,22-25]. For example, GP zones nucleate in the 7050 Al alloy during one pass of ECAP at room temperature and it was shown that the presence of these ordered phases, allied with the high density of dislocations after ECAP processing, accelerates the nucleation and growth of η' and η precipitates during post-ECAP aging at 433 K

for 60 h [22]. There is also a report that the needle-like precipitates in an AA6060 alloy were fragmented during ECAP processing up to 8 passes and numerous small precipitates were dispersedly distributed after ECAP for 2 passes and subsequent aging [23].

In practice, dispersoids have different thermal stabilities and pinning capabilities according to their sizes and coherency with the Al matrix. For example, the Cr-rich phase in a 7075 Al alloy was thermally stable while the Mg-Zn particles gradually coarsened with increasing numbers of passes during processing by accumulative roll bonding (ARB) [24]. Another report showed that the high density of $Al_{20}Cu_2Mn_3$ precipitates in an Al-Cu-Li alloy processed by hot rolling was unable to provide sufficient pinning forces to prevent the migration of grain boundaries during post-deformation heat treatment at 808 K by comparison with the Al_3Zr dispersoids [25]. The lower pinning forces provided by the Mn-rich phase in relation to the Zr-rich particles is attributed to its relatively lower coherency with the Al matrix, its higher aspect ratio and its larger size [25]. A review of these data shows that the high strains imposed by SPD processing are able to increase the precipitation rate and the refinement of different phases. However, it is not clear whether different phases in the Al-Zn-Mg alloy, including the $MgZn_2$ (η', η), Cr and Mn-rich (E and T) phases, are able to provide a thermally stable structure during post-ECAP annealing. In addition, the influence of post-ECAP annealing on the interactions among these different phases is also not clear. It is concluded, therefore, that a more complete understanding of the precipitation behavior during ECAP and post-ECAP annealing is needed in order to successfully tailor the precipitation in Al-Zn-Mg alloys and thereby achieve optimum properties.

The present investigation was initiated specifically to study the formation and distribution of different types of precipitates in an Al-Zn-Mg alloy during processing by ECAP and after

post-ECAP annealing. The effect of these phases on the grain stability was also examined at temperatures up to 473 K in order to evaluate the potential for applying UFG Al-Zn-Mg alloys in high temperature environments.

2. Experimental material and procedures

The experiments were conducted using an Al-Zn-Mg alloy bought from Shanghai Silu Metal Materials Co.Ltd. having a chemical composition, in wt.%, of Al-4.53 Zn-2.52 Mg-0.35 Mn-0.2 Cr-0.11 Cu-0.1 Zr received after solid solution processing at 743 K for 1 h and aging at 393 K for 24 h. Billets of the as-received material with diameters of 9.8 mm and lengths of 65 mm were processed by 4 or 8 ECAP passes using a solid die having an internal channel angle of 90° and an outer arc of curvature of 20°. These angular values impose an equivalent strain of ~1 in each pass [26] and the ECAP processing was performed at 423 K using route B_c where the billet is rotated by 90° in the same sense between each pass [27]. The ECAP was conducted at 423 K to avoid problems with cracking at lower temperatures [13, 28, 29]. There is experimental evidence that the temperature of the billet increases during the pressing operation [30-32] and, using the available data, this temperature rise was estimated as ~18 K for a pressing of 30 s.

Following ECAP processing, samples of the Al-Zn-Mg alloy were annealed at 393 K or 473 K for 20 h using a forced convection furnace and then cooled in air. A pictorial description of the heat treatment and processing sequence of the Al-Zn-Mg alloy is given in Fig. 1.

Phase identification and microstructural observations were performed using transmission electron microscopy (TEM) with an FEI Tecnai G2 F20 X-TWIN equipped with a scanning unit and an energy-dispersive (EDS) detector operating at 200 kV. The samples for TEM were prepared by electro-polishing in an electrolyte of 8% perchloric acid and 92% ethanol at 248 K using a voltage of 22 V and a current of ~40 mA. After the electro-polishing, the samples were

further thinned by ion-milling (Leica RES 101) at 3 kV using a current of 1 mA for 30 min and removing any possible contamination caused by electro-polishing. Samples for energy-dispersive X-ray (EDX) analysis were subjected to additional surface cleaning using Ar/O_2 gas chemistry with a Gatan Plasma cleaning system. Particle size measurements were conducted in scanning transmission electron microscopy (STEM) mode using a high-angle annular dark field detector (HAADF). The average particle size was measured by calculating the mean of ~400 particles in each condition [33]. The average grain sizes of the samples were measured with the aid of TEM and STEM images by counting more than 150 intercepts using the Circular intercept method following ASTM E112-12 [34]. In order to quantify the density and volume fraction of precipitates, the foil thickness measurements were performed with the aid of convergent beam electron diffraction (CBED). The TEM region was tilted to obtain a two-beam condition with a dark Kikuchi line crossing the 000_{Al} bright disk and a bright Kikuchi line crossing the 220_{Al} dark disk in the CBED. A detail description on the thickness determination is given elsewhere [35].

3. Experimental results

3.1 Characterization of the precipitates after ECAP processing

HAADF-STEM images of the as-received and the ECAP-processed Al-Zn-Mg alloy viewed along the $<114>_{Al}$ zone axis are displayed in Fig. 2. The different phases visible in Fig. 2 were identified through EDX analysis and detailed structural information is shown in Table 1 [36-39]. The average grain size of the as-received Al-Zn-Mg alloy was ~1.3 μm and this was refined to ~200 nm after 4 passes and ~190 nm after 8 passes of ECAP, respectively [40]. It is apparent from Fig. 2 (a) that plate and spherical-like second phase particles are heterogeneously distributed within the microstructure of the as-received alloy. Precipitates mainly of the η' phase were detected with the presence of a few η, T and E precipitates along the grain boundaries and

within the grains of the material in the as-received condition as shown in Fig. 2 (d). Overlapping of some precipitates was observed which may originate from coarsening during the aging treatment. The fine η' precipitates were mainly at the grain boundaries and had an average size of ~120 nm whereas the T and E phases were of the order of ~180 nm.

Figure 2 (b) shows that the sizes of the T and E phases are reduced and more η precipitates form after 4 passes of ECAP by comparison with the unprocessed material. Fig. 2 (e) is a selected area at higher magnification in Fig. 2 (b) and it shows η, T and E precipitates of ~60 nm as well as numerous fine η' precipitates which are uniformly distributed. The amount of precipitation further increases by increasing the number of ECAP passes from 4 to 8, as shown in Fig. 2 (c) and (f). The presence of spherical precipitates of the η, T and E phases having an average size of ~65 nm together with homogeneous fine η' is apparent in Fig. 2 (f). Furthermore, the η phase was identified within some T and E phases after ECAP in Fig. 2 (e) and (f). Table 2 shows EDX results of selected T and E phases and it reveals a decrease in the content of Mn and Cr, which are the T and E forming elements, accompanied by an increase of Mg and Zn, which are the η forming elements, with increasing numbers of ECAP passes. This indicates that the E and T phases are refined and begin to dissolve to form η phase [41] as is readily visible in Fig. 3 which depicts EDX maps of the Al-Zn-Mg alloy after ECAP for 4 passes showing an E phase along a grain boundary containing fine η precipitates.

In order to investigate the Al_3Zr dispersoid evolution during ECAP processing, Fig. 4 shows TEM and selected area electron diffraction (SAED) images of the Al-Zn-Mg alloy in the as-received condition and after 4 and 8 passes of ECAP. The SAED patterns were taken along the $<110>_{Al}$ zone axis of the as-received material and they contain weak spots of Al_3Zr at 1/2 of {220} as shown in Fig. 4 (a) [42]. After 4 and 8 ECAP passes, Al_3Zr dispersoid spots are also

observed at 1/2 of {220} as displayed in Figs 4 (b) and 4 (c), respectively. This suggests that there is a small quantity of nano-scaled Al_3Zr dispersoids in the microstructure of the Al-Zn-Mg alloy and these fine precipitates remain stable during the ECAP processing.

3.2 Characterization of the precipitates after post-ECAP annealing

The HAADF-STEM images in Fig 5 display the distributions of second phase particles in the Al alloy processed by ECAP and further heat treated for 20 h at 393 K or 473 K taken along the $<100>_{Al}$ zone axes. The bright field TEM along $<110>_{Al}$ in Fig. 6 shows the grain structure after post-ECAP annealing. It is readily apparent from these images that there are large precipitates mostly distributed along the grain boundaries after post-ECAP annealing together with very fine particles evenly distributed within the grains. Inspection of Fig. 5 (a) shows many fine spherical η' and η precipitates with average sizes of ~13.5 nm in the grains and mainly of T and E precipitates with diameters of ~82 nm along the grain boundaries after 4 ECAP passes and further annealing at 393 K for 20 h. Fig. 6 (a) shows that the microstructure of the alloy has fine equiaxed grains of ~ 230 nm in size. Increasing the annealing temperature to 473 K for the Al-Zn-Mg alloy processed by 4 ECAP passes produces a slight increase in grain size and a slight coarsening of the phases by comparison with the material heat treated at 393 K. The size of the grains in Fig. 6 (b) is ~240 nm and the mean size of the precipitates in the grains is ~21 nm but this value is ~114 nm along the grain boundaries as depicted in Fig. 5 (b).

After ECAP processing for 8 passes and annealing at 393 K for 20 h, a higher area fraction of fine precipitates homogeneously distributed within the microstructure was observed in the micrograph shown in Fig. 5 (c) by comparison with Fig. 5 (a). Spherical precipitates with average size of ~14 nm were distributed in the grains together with larger grain along the grain boundaries with size of ~76 nm. Fig. 6 (c) displays fine grains with mean sizes of ~210 nm. The

Al-Zn-Mg alloy processed by 8 passes of ECAP and further annealed at 473 K exhibited plate-like precipitates along the grain boundaries, mostly of the T, E and η phases, with lengths of ~140 nm together with a high fraction of fine η' and η precipitates having an average size of ~ 11 nm uniformly distributed in the Al matrix with a grain size of ~230 nm as shown in Figs 5 (d) and 6 (d). A comparison of the grain size before and after post-ECAP annealing at 393 and 473 K for 20h reveals small variations which demonstrate that second phase particles are capable of hindering grain growth during the heat treatments. The volume fraction of the particles after post-ECAP heat treatments was evaluated following standard procedures [43]. It is 0.085, 0.095 and 0.089 in the microstructure after 4 passes of ECAP followed by annealing at 393 K, at 473 K and after 8 passes of ECAP followed by annealing at 393 K, respectively. For the 8 passes followed by annealing at 473 K, precipitates are spherical and there are platelet morphologies. The volume fraction of the spherical precipitates is ~0.072 and ~0.019 for the platelet precipitates. Table 3 presents a summary of the microstructural features in the as-received material, after ECAP and after post-ECAP heat treatments.

Figure 7 shows an EDX map in which two η phases having irregular shapes with a mean size of ~20 nm are located at the edges of a Mn-rich precipitate with a triangular morphology. The ratio of Zn:Mg detected by EDX was ~2:1 which is in agreement with the composition of the Laves phase $MgZn_2$ and the Al-Zn-Mg phase diagram [44]. In addition, EDX composition plots of the Mn and Cr phases and their average compositions are depicted in Fig. 8. These plots display the percentage of Zn (wt%) detected from the interior of the phases in the post-ECAP heat-treated Al-Zn-Mg alloy. Each point in Fig. 8 represents the Zn content in a randomly selected precipitate. By comparing Fig. 8 (a) with Fig. 8 (b), it is apparent that the Zn (wt%) content in the $Al_{18}Mg_3Cr_2$ phase (the E phase) increases with increasing annealing temperature.

Furthermore, the results also show that the Cr (wt%) content decreases as a result of the increasing wt% of Mg and Zn. This may follow from the decomposition of the $Al_{18}Mg_3Cr_2$ precipitate (E phase) to form $MgZn_2$ (η phase). Similarly, Fig. 8 (c) and 8 (d)) shows that the Zn (wt%) in the $Al_{18}Cu_2Mn_3$ precipitates increases at the expense of the wt% Mn and Cu which also indicates that the $Al_{18}Cu_2Mn_3$ (T phase) starts to decompose and form $MgZn_2$ (η phase) in the grain interior. Additionally, it should be noted that the Zn (wt%) was slightly higher after the post-ECAP heat treatment in the material processed earlier by a larger number of ECAP passes.

Figure 9 shows high magnification TEM micrographs and SAED patterns revealing the presence of Al_3Zr dispersoids within the microstructure of the Al-Zn-Mg alloy processed by ECAP and further heat treated at 473 K for 20 h. The SAED pattern along the $<110>_{Al}$ zone axis shows spots of Al_3Zr oriented at 1/2 {200} in Fig. 9 (a) and slightly outside 1/2 {220} in Fig. 9 (b). There remain very few Al_3Zr dispersoids within the matrix after the post-ECAP heat treatments. Inspection of Figs 4 and 9, demonstrates that these dispersoids are thermally stable displaying a spherical shape with a diameter of ~12 nm as marked by black arrows in Fig. 9. In addition, through observations of the microstructure by TEM, it was found there are twins within some T and E precipitates as is apparent in Fig. 9 (b).

3.3 Overlapping of the phases

Overlapping of different phases was observed in the Al-Zn-Mg alloy in the as-received condition and after post-ECAP annealing. Fig. 10 shows a sequence of HRTEM images revealing the overlapping process in the Al alloy processed by 4 ECAP passes and further heat treated at 393 K. In Fig. 10 (a), two E phases overlap with a T phase observed close to an array of dislocations. Fine η precipitates are also evident within the T phase with a size of ~12 nm as shown in Fig. 10 (b). The highlighted lattice fringes in Fig. 10 (c) show a mismatch of the lattice

planes between the two different phases. The FFT patterns displayed in Fig. 10 (d) display the T and E phase planes with the presence of η phase along $(201)_{Al}$.

3.4 Twinning of precipitates

Twinning is observed in the material processed by 8 passes of ECAP and further heat treated at 393 K as depicted in Fig. 11. Fig. 11 (a) shows twinning planes in an E phase which overlaps with a T phase and Fig. 11 (b) displays clear twinning planes along {112} in the E phase. The FFT patterns display the extra spots of the twinning plane in addition to the reflection planes of the coalesced phases. Fig. 11 (c) is a selected IFFT and clearly confirms the presence of dislocation pairs within the twinning while groups of dislocations are visible in Figs. 11 (d) and (e). The presence of these dislocations supports the proposal that the twins originate from the dissociation of dislocations [45].

4. Discussion

4.1 Precipitate evolution during ECAP

In the present investigation, a low number of heterogeneous T and E phases were detected by EDX in the as-received Al-Zn-Mg alloy. These precipitates have spherical and plate-like shapes in two-dimensional projections as shown in Fig. 2 (a). Because of the large plastic straining during ECAP, the precipitates are fragmented, refined and begin to dissolve in the Al matrix [46]. Accordingly, the presence of fine-scale and homogeneously distributed spherical η' precipitates after 4 passes of ECAP may result from the occurrence of fragmentation during the ECAP processing [47]. Increasing the numbers of ECAP passes to 8 leads to the formation of a larger quantity of spherical η' and η phase [48].

During ECAP processing, the high density of mobile dislocations serves as fast diffusion paths for solute atoms in the fragmented precipitates [49]. Consequently, the η phase detected

within the E and T phases as in Table 2 and Fig. 3 can be attributed to dislocation glide during straining. In related studies, it was reported that the excess energy from the solute-core interactions and the relatively open structure of the cores promotes solute diffusion along the dislocation cores [50,51]. Very few Al_3Zr dispersoids were observed in the Al-Zn-Mg alloy in the as-received and ECAP-processed conditions. Furthermore, the fine scale Al_3Zr dispersoids produced through the aging treatment in the as-received material remain essentially unaffected after ECAP processing due to a the relatively large solubility limit of Zr in Al of 0.14 wt.% [52,53].

4.2 Precipitate evolution during post-ECAP annealing

Micrographs of the Al-Zn-Mg alloy after processing by ECAP for 4 passes and heat treatment at 393 K for 20 h show high amounts of T, E, spherical η and η' phases as is apparent by inspection of Figs 5 and 6. The presence of very fine precipitates after heating at 393 K may be ascribed to the precipitation of the dissolved solutes after ECAP processing which forms newly fine-scale and uniformly distributed particles. Precipitate dissolution during SPD and the nucleation of precipitates after post-SPD heat treatments were observed in binary Al alloys such as Al-Cu and Al-Mg [54,55]. Increasing the post-ECAP annealing temperature in the Al alloy processed by 4 ECAP passes to 473 K leads to a slight coarsening of precipitates. For the material processed by 8 passes of ECAP, the size and amount of precipitation increases after heating. The increased number of precipitates is due to the rise of the stored energy after ECAP processing for 8 passes which leads to an increase of the diffusion rate during the heating process and subsequently to an increase in the fraction of precipitates [56]. The presence of twin planes within some precipitates is a direct consequence of the subsequent thermal instability and coarsening during heating [57, 58]. Fig. 11 displays the dissociation of dislocations to twinning

in an E precipitate where groups of dislocations were able to provide cross-slip. The twin planes are bounded with dislocations along {112} [59]. The presence of dislocations on both twin boundaries supports the proposal that these dislocations transform into stacking faults and then twinning is produced with further heating through the coalescence of these faults. The presence of a dislocation pair within the twinning planes as in Fig. 11 (c) supports the theory of the multiplication of faults [60]. The higher density of dislocations in the Al-Zn-Mg alloy processed by 8 passes of ECAP leads to the presence of more twin planes within the precipitates after heating by comparison with the material processed by 4 ECAP passes as shown in Fig. 9 [40].

It is also revealed in the current study that precipitates positioned along the grain boundaries are coarser in size and this may lead to some overlapping. During the precipitation process near grain boundaries, solute atoms diffuse towards the grain boundaries through volume diffusion, they move along the boundaries to the precipitates and then they are deposited over the surface of the growing particles through interfacial diffusion [61]. Thus, the growth rates of the particles at grain boundaries are higher than within the grains and some of these particles have irregular shapes after overlapping. By contrast, the few Al_3Zr dispersoids observed after ECAP processing were thermally stable after further heat treatments as these dispersoids have an Ll_2 structure which is thermally stable up to 698 K [62].

Precipitates of the η phase are evident within the T and E phases after post-ECAP heat treatments. This may be ascribed to the permanence of η precipitates within these phases from the ECAP-processed metal or to their nucleation during post-ECAP annealing. The presence of atomic disorder associated with the grain boundaries contributes to the reduction of the activation energy barrier for nucleation and this accelerates the precipitation kinetics. Therefore, grain boundaries act as preferable sites for heterogeneous nucleation of precipitates [63].

Accordingly, the T and E phases along the grain boundaries are favorable sites for the heterogeneous nucleation of η phases during post-ECAP heat treatments as is evident in Fig. 7.

4.3 The effect of precipitates on grain size

The average pinning force applied by the precipitates on the moving boundaries during grain growth, *Z*, may be estimated through the relationship [64]

$$Z = k\left(\frac{f\gamma}{r}\right) \qquad (1)$$

where k is a scaling factor (1.5 for spherical particles [25]), γ is the energy of the boundary pinned by the precipitates, 0.32 J m^{-2} for the alloy [65], r is the mean radius of the precipitates, and f is the volume fraction of the particles. Substituting of r and f obtained in the results into Eq. (1) gives $Z \approx 0.544 \times 10^6$ Nm^{-2} , 0.48×10^6 Nm^{-2} and 0.65×10^6 Nm^{-2} after ECAP processing for 4 passes and subsequent annealing for 20 h at 393 and 473 K and after 8 ECAP passes followed by annealing for 20 h at 393K, respectively. For 8 passes and annealing at 473 K, the Z value is a combination of the spherical and platelet morphologies. For the spherical precipitates, the pinning force is 0.42×10^6 Nm^{-2}. The equation for the pinning force by plate precipitates [66] gives $\sigma_s \varepsilon^{0.47}$ where σ_s is the force exerted by a sphere of the same volume and ε is the aspect ratio of the particle (length/width). By calculation, the pinning force provided by the plate particles is 0.2×10^6 Nm^{-2}.It follows from Eq. (1) that the Zener pinning force increases by increasing the volume fraction (*f*) and decreasing the particle size (*r*). There is a small variation in the grain size before and after heat treatment at 393 and 473 K for 20 h. The coarsening of precipitates along the grain boundaries in the post-ECAP annealed alloy at 473 K has no significant influence on the *Z* values. This is attributed to the increase in the number of fine η' precipitates during heating at 473 K which sufficiently compensates for the decrease in the pinning force values due to the increase in size of the remaining phases. Overall, the grain structures of the UFG Al-Zn-Mg

alloy display only a slight coarsening after heating up to 473 K for 20 h and the microstructural stability of the ECAP-processed material is further improved by the presence of fine precipitates which effectively impede grain boundary migration during any long-term heat treatment.

5. Summary and conclusions

1. During 4 passes of ECAP processing for an Al-Zn-Mg alloy with precipitates of ~120 nm, the η' , η, T and E phases are fragmented into groups of fine spherical particles having average sizes of ~ 60 nm. Increasing the numbers of passes to 8 increases the numbers of these precipitates and increases their average size to ~ 65 nm.

2. After post-ECAP annealing at 393 and 473 K for 20 h, the precipitates in the microstructure consist of larger particles mostly distributed along the grain boundaries and finer particles distributed evenly within the grains. Increasing the ECAP passes from 4 to 8 leads to an increase in the quantity of the finer precipitates. Increasing the annealing temperature from 393 to 473 K produces slight coarsening of the precipitates for 4 passes of ECAP but there is greater coarsening after 8 passes of ECAP.

3. There are a few Al_3Zr dispersoids in the as-received material and after ECAP and the post-ECAP heat treatments. These dispersoids are thermally stable during the heat treatments and display fine spherical morphology.

4. Due to dislocation motion during ECAP processing, the η phase is nucleated within the T and E phases where these dislocations act as a fast diffusion path for solute atoms. During post-ECAP heat treatments, the η phase is also promoted for nucleation in the T and E phases

Acknowledgements

This work was supported by the National Natural Science Foundation of China under Grants nos. 51671030 and 11521062, the Brazilian Federal Agency for the Support and Evaluation of Graduate Education (CAPES) and the European Research Council under ERC Grant Agreement no. 267464-SPDMETALS.

References

[1] C.M. Cepeda-Jiménez, J.M. García-Infanta, O.A. Ruano, F. Carreño, High strain rate superplasticity at intermediate temperatures of the Al 7075 alloy severely processed by equal channel angular pressing, J. Alloys Compd. 509 (2011) 9589-9597. doi:10.1016/j.jallcom.2011.07.076.

[2] D. Xu, Z. Li, G. Wang, X. Li, X. Lv, Y. Zhang, Y. Fan, B. Xiong, Phase transformation and microstructure evolution of an ultra-high strength Al-Zn-Mg-Cu alloy during homogenization, Mater. Charact. 131 (2017) 285-297. doi:10.1016/j.matchar.2017.07.011.

[3] T.G. Langdon, Twenty-five years of ultrafine-grained materials: achieving exceptional properties through grain refinement, Acta Mater. 61 (2013) 7035–7059.

[4] M. Furukawa, Z. Horita, M. Nemoto, R. Z. Valiev, T.G. Langdon, Microhardness measurements and the hall-petch relationship in an Al–Mg alloy with submicrometer grain size, Acta Mater. 44 (1996) 4619-4629. doi: 10.1016/1359-6454(96)00105-X.

[5] A. Veveçka, M. Cabibbo, T.G. Langdon, A characterization of microstructure and microhardness on longitudinal planes of an Al-Mg-Si alloy processed by ECAP, Mater. Charact. 84 (2013) 126-133. doi: 10.1016/j.matchar.2013.07.016.

[6] R.Z. Valiev, T.G. Langdon, Principles of equal-channel angular pressing as a processing tool for grain refinement, Prog. Mater Sci. 51 (2006) 881-981. doi:10.1016/j.pmatsci.2006.02.003.

[7] Y. Iwahashi, Z. Horita, M. Nemoto and T.G. Langdon, An investigation of microstructural evolution during equal-channel angular pressing, Acta Mater. 45 (1997) 4733-4741. doi:10.1016/S1359-6454(97)00100-6.

[8] P. Málek, M. Cieslar, R.K. Islamgaliev, The influence of ECAP temperature on the stability of Al-Zn-Mg-Cu alloy, J. Alloys Compd. 378 (2004) 237-241.doi:10.1016/j.jallcom.2003.11.161.

[9] L.J. Zheng, C.Q. Chen, T.T. Zhou, P.Y. Liu, M.G. Zeng, Structure and properties of ultrafine-grained Al-Zn-Mg-Cu and Al-Cu-Mg-Mn alloys fabricated by ECA pressing combined with thermal treatment, Mater. Charact. 49 (2002) 455-461. doi: 10.1016/S1044-5803(03)00069-X.

[10] R. Gürbüz, S.P. Alpay, The effect of coarse second phase particles on fatigue crack propagation of an Al-Zn-Mg-Cu alloy, Scripta Metall. Mater. 30 (1994) 1373-1376. doi: 10.1016/0956-716X(94)90230-5.

[11] M. Dixit, R.S. Mishra, K.K. Sankaran, Structure–property correlations in Al 7050 and Al 7055 high–strength aluminum alloys, Mater. Sci. Eng. A 478 (2008) 163-172. doi:10.1016/j.msea.2007.05.116.

[12] J. Gubicza, I. Schiller, N.Q. Chinh, J. Illy, Z. Horita, T.G. Langdon, The effect of severe plastic deformation on precipitation in supersaturated Al-Zn-Mg alloys, Mater. Sci. Eng. A 460-461 (2007) 77-85. doi:10.1016/j.msea.2007.01.001.

[13] M.H. Shaeri, M. Shaeri, M. Ebrahimi, M.T. Salehi, S.H. Seyyedein, Effect of ECAP temperature on microstructure and mechanical properties of Al-Zn-Mg-Cu alloy, Prog. Nat. Sci. Mater. Int. 26 (2016) 182-191. doi:10.1016/j.pnsc.2016.03.003.

[14] S.R. Kumar, K. Gudimetla, P. Venkatachalam, B. Ravisankar, K. Jayasankar, Microstructural and mechanical properties of Al 7075 alloy processed by equal channel angular pressing, Mater. Sci. Eng. A 533 (2012) 50-54. doi:10.1016/j.msea.2011.11.031.

[15] I. Mazurina, T. Sakai, H. Miura, O. Sitdikov, R. Kaibyshev, Grain refinement in aluminum alloy 2219 during ECAP at 250°C, Mater. Sci. Eng., A 473 (2008) 297-305. doi:10.1016/j.msea.2007.04.112.

[16] R. Kaibyshev, O. Sitdikov, A. Goloborodko, T. Sakai, Grain refinement in as-cast 7475 aluminum alloy under hot deformation, Mater. Sci. Eng. A 344 (2003) 348-356. doi:10.1016/S0921-5093(02)00440-9.

[17] A. Goloborodko, O. Sitdikov, R. Kaibyshev, H. Miura, T. Sakai, Effect of pressing temperature on fine-grained structure formation in 7475 aluminum alloy during ECAP, Mater. Sci. Eng., A 381 (2004) 121-128. doi:10.1016/j.msea.2004.04.049.

[18] O. Sitdikov, T. Sakai, E. Avtokratova, R. Kaibyshev, Y. Kimura, K. Tsuzaki, Grain refinement in a commercial Al-Mg-Sc alloy under hot ECAP conditions, Mater. Sci. Eng. A 444 (2007) 18-30. doi:10.1016/j.msea.2006.06.081.

[19] O. Sitdikov, T. Sakai, A. Goloborodko, H. Miura, Grain fragmentation in a coarse-grained 7475 Al alloy during hot deformation, Scripta Mater. 51 (2004) 175-179. doi:10.1016/j.scriptamat.2004.02.034.

[20] O. Sitdikov, T. Sakai, A. Goloborodko, H. Miura, R. Kaibyshev, Grain refinement in coarse-grained 7475 Al alloy during severe hot forging, Philos. Mag. 85 (2005) 1159-1175. doi:10.1080/14786430412331325049.

[21] C. Xu, M. Furukawa, Z. Horita, T.G. Langdon, Using ECAP to achieve grain refinement, precipitate fragmentation and high strain rate superplasticity in a spray-cast aluminum alloy, Acta Mater. 51 (2003) 6139–6149. doi:10.1016/S1359-6454(03)00433-6.

[22] M.H. Li, Y.Q. Yang, Z.Q. Feng, G.H. Feng, B. Huang, Y.X. Chen, M. Han, J.G. Ru, Influence of equal-channel angular pressing on aging precipitation in 7050 Al alloy, Intermetallics 55 (2014) 49–55. doi:10.1016/j.intermet.2014.07.005.

[23] K. Hockauf, M.F.-X Wagner, T. Halle, T. Niendorf, M. Hockauf, T. Lampke, Influence of precipitates on low-cycle fatigue and crack growth behavior in an ultrafine-grained aluminum alloy, Acta Mater. 80 (2014) 250-263. doi:10.1016/j.actamat.2014.07.061.

[24] P. Hidalgo-Manrique, C.M. Cepeda.-Jiménez, A. Orozco.-Caballero, O.A. Ruano, F. Carreño, Evolution of the microstructure, texture and creep properties of the 7075 aluminium alloy during hot accumulative roll bonding, Mater. Sci. Eng. A 606 (2014) 434-442. doi:10.1016/j.msea.2014.03.105.

[25] D. Tsivoulas, P.B. Prangnell, The effect of Mn and Zr dispersoid–forming additions on recrystallization resistance in Al-Cu-Li AA2198 sheet, Acta Mater. 77 (2014) 1-16. doi:10.1016/j.actamat.2014.05.028.

[26] Y. Iwahashi, J. Wang, Z. Horita, M. Nemoto, T.G. Langdon, Principle of equal-channel angular pressing for the processing of ultra-fine grained materials, Scripta Mater. 35 (1996) 143-146. doi: 10.1016/1359-6462(96)00107-8.

[27] M. Furukawa, Y. Iwahashi, Z. Horita, M. Nemoto, T.G. Langdon, The shearing characteristics associated with equal-channel angular pressing, Mater. Sci. Eng. A 257 (1998) 328-332. doi:10.1016/S0921-5093(98)00750-3.

[28] I. Schiller, J. Gubicza, Z. Kovács, N.Q. Chinh, J. Illy, Precipitation and Mechanical Properties of Supersaturated Al-Zn-Mg Alloys Processed by Severe Plastic Deformation, Mater. Sci. Forum. 519–521 (2006) 835–840. doi:10.4028/www.scientific.net/MSF.519-521.835.

[29] Z. Horita, T. Fujinami, M. Nemoto, T.G. Langdon, Equal-Channel Angular Pressing of Commercial Aluminum Alloys: Grain Refinement, Thermal Stability and Tensile Properties, Metall. Mater. Trans. A 31 (2000) 691–701. doi: 10.1007/s11661-000-0011-8.

[30] D. Yamaguchi, Z. Horita, M. Nemoto, T.G. Langdon, Significance of adiabatic heating in equal-channel angular pressing, Scr. Mater. 41 (1999) 791–796. doi:10.1016/S1359-6462(99)00233-X.

[31] Y. Nishida, T. Ando, M. Nagase, S.W. Lim, I. Shigematsu, A. Watazu, Billet temperature rise during equal-channel angular pressing, Scr. Mater. 46 (2002) 211–216. doi:10.1016/S1359-6462(01)01226-X.

[32] Q.X. Pei, B.H. Hu, C. Lu, Y.Y. Wang, A finite element study of the temperature rise during equal channel angular pressing, Scr. Mater. 49 (2003) 303–308. doi:10.1016/S1359-6462(03)00284-7.

[33] M. T. Shehata, Practical Guide to Image Analysis, ASM International, Materials Park, 2000, pp. 129-143.

[34] H. Abrams, Grain size measurement by the intercept method, Metallography 4 (1971) 59–78. doi:10.1016/0026-0800(71)90005-X.

[35] David B. Williams, C. Barry Carter, Transmission Electron Microscopy A Textbook for Materials Science, Springer, New York, 2009.

[36] W. B. Pearson, A Handbook of Lattice Spacings and Structures of Metals and Alloys, Pergamon Press, Oxford, 1958.

[37] X.Z. Li, V. Hansen, J. Gjønnes, L.R. Wallenberg, HREM study and structure modeling of the η' phase, the hardening precipitates in commercial Al-Zn-Mg alloys, Acta Mater. 47 (1999) 2651-2659. doi:10.1016/S1359-6454(99)00138-X.

[38] S.K. Maloney, K. Hono, I.J. Polmear, S.P. Ringer, The chemistry of precipitates in an aged Al–2.1Zn–1.7Mg at.% alloy, Scripta Mater. 41 (1999) 1031-1038. doi:10.1016/S1359-6462(99)00253-5.

[39] S.R. Ortner, C.R.M. Grovenor, B.A. Shollock, On the structure and composition of G–P zones in high purity AlZnMg alloys, Scripta Metall. 22 (1988) 839–842. doi:10.1016/S0036-9748(88)80060-7.

[40] M.A. Afifi, P.H.R. Pereira, Y.C. Wang, Y. Wang, S. Li, T.G. Langdon, Effect of ECAP processing on microstructure evolution and dynamic compressive behavior at different temperatures in an Al-Zn-Mg alloy, Mater. Sci. Eng. A 684 (2017) 617-625. doi: 10.1016/j.msea.2016.12.099.

[41] S.T. Lim, S.J. Yun, S.W. Nam, Improved quench sensitivity in modified aluminum alloy 7175 for thick forging applications, Mater. Sci. Eng. A 371 (2004) 82-90. doi:10.1016/S0921-5093(03)00653-1.

[42] A. Deschamps, Y. Bréchet, Influence of quench and heating rates on the ageing response of an Al-Zn-Mg-(Zr) alloy, Mater. Sci. Eng. A 251 (1998) 200-207. doi:10.1016/S0921-5093(98)00615-7.

[43] G.A. Botton, G. L'Espérance, C.E. Gallerneault, M.D. Ball, Volume fraction measurement of dispersoids in a thin foil by parallel energy-loss spectroscopy : development and assessment of the technique, J. Microsc. 180 (1995) 217-229. doi: 10.1111/j.1365-2818.1995.tb03681.x.

[44] R. Howard, N. Bogh, D. S. MacKenzie, Heat Treating Processes and Equipment, in: G. E. Totten, D. S. MacKenzie (Eds.), Handbook of Aluminum Volume 1 Physical Metallurgy and Processes, Marcel Dekker, New York, 2003, 911-920.

[45] K. Ogawa, Edge dislocations dissociated in {112} planes and twinning mechanism of B.C.C. metals, Philos. Mag. 11 (1965) 217-233. doi:10.1080/14786436508221852.

[46] M. Murayama, Z. Horita, K. Hono, Microstructure of two–phase Al-1.7 at% Cu alloy deformed by equal-channel angular pressing, Acta Mater. 49 (2001) 21-29. doi:10.1016/S1359-6454(00)00308-6.

[47] G. Sha, Y.B. Wang, X.Z. Liao, Z.C. Duan, S.P. Ringer, T.G. Langdon, Influence of equal-channel angular pressing on precipitation in an Al-Zn-Mg-Cu alloy, Acta Mater. 57 (2009) 3123-3132. doi:10.1016/j.actamat.2009.03.017.

[48] M.H. Shaeri, M.T. Salehi, S.H. Seyyedein, M.R. Abutalebi, J.K. Park, Microstructure and mechanical properties of Al–7075 alloy processed by equal channel angular pressing combined with aging treatment, Mater. Des. 57 (2014) 250–257. doi:10.1016/j.matdes.2014.01.008.

[49] T. Hu, K. Ma, T.D. Topping, J.M. Schoenung, E.J. Lavernia, Precipitation phenomena in an ultrafine-grained Al alloy, Acta Mater. 61 (2013) 2163-2178. doi:10.1016/j.actamat.2012.12.037.

[50] R.B. Schwarz, Microscopic model for mechanical alloying, Mater. Sci. Forum. 269-272 (1998) 665–674. doi:10.4028/www.scientific.net/MSF.269-272.665.

[51] M. Legros, G. Dehm, E.Arzt, T. J. Balk, Observation of giant diffusivity along dislocation cores, Sci. 319 (2008) 1646-1649. doi:10.1126/science.1151771.

[52] I. Nikulin, A. Kipelova, S. Malopheyev, R. Kaibyshev, Effect of second phase particles on grain refinement during equal–channel angular pressing of an Al-Mg-Mn alloy, Acta Mater. 60 (2012) 487-497. doi:10.1016/j.actamat.2011.10.023.

[53] Y.W. Riddle, T.H. Sanders Jr, A study of coarsening, recrystallization, and morphology of microstructure in Al-Sc-(Zr)-(Mg) alloys, Metall. Mater. Trans. A 35 (2004) 341-350. doi:10.1007/s11661-004-0135-3.

[54] W. Huang, Z. Liu, M. Lin, X. Zhou, L. Zhao, A. Ning, S. Zeng, Reprecipitation behavior in Al–Cu binary alloy after severe plastic deformation–induced dissolution of θ' particles, Mater. Sci. Eng. A 546 (2012) 26-33. doi:10.1016/j.msea.2012.03.010.

[55] M.A. Muñoz-Morris, C. Garcia Oca, D.G. Morris, Mechanical behaviour of dilute Al-Mg alloy processed by equal channel angular pressing, Scripta Mater. 48 (2003) 213-218. doi:10.1016/S1359-6462(02)00501-8.

[56] T. Fujita, Z. Horita, T.G. Langdon, Using grain boundary engineering to evaluate the diffusion characteristics in ultrafine–grained Al-Mg and Al-Zn alloys, Mater. Sci. Eng. A 371 (2004) 241-250. doi:10.1016/j.msea.2003.12.042.

[57] C.W.T. Bulle-Lieuwma, A.H. van Ommen, L.J. van Ijzendoorn, Microstructure of heteroepitaxial Si/$CoSi_2$/Si formed by Co implantation into (100) and (111) Si, Appl. Phys. Lett. 54 (1989) 244-246. doi:10.1063/1.101446.

[58] F. Czerwinski, A. Zielinska-Lipiec, The melting behaviour of extruded Mg-8%Al-2%Zn alloy, Acta Mater. 51 (2003) 3319-3332. doi:10.1016/S1359-6454(03)00163-0.

[59] S. Mahajan, Interrelationship between slip and twinning in B.C.C crystals, Acta Metall. 23 (1975) 671-684. doi:10.1016/0001-6160(75)90049-8.

[60] J.W. Christian, S. Mahajan, Deformation twinning, Prog. Mater Sci. 39 (1995) 1-157. doi:10.1016/0079-6425(94)00007-7.

[61] A.D. Brailsford, H.B. Aaron, Growth of grain-boundary precipitates, J. Appl. Phys. 40 (1969) 1702-1710. doi:10.1063/1.1657835.

[62] K.E. Knipling, D.C. Dunand, D.N. Seidman, Precipitation evolution in Al-Zr and Al-Zr-Ti alloys during aging at 450–600 °C, Acta Mater. 56 (2008) 1182-1195. doi:10.1016/j.actamat.2007.11.011.

[63] A. Fillon, X. Sauvage, A. Pougis, O. Bouaziz, D. Barbier, R. Arruffat, L.S. Toth, Influence of severe plastic deformation on the precipitation hardening of a FeSiTi steel, J. Mater. Sci. 47 (2012) 7939-7945. doi:10.1007/s10853-012-6536-6.

[64] V. Randle, B. Ralph, Interactions of grain boundaries with coherent precipitates during grain growth, Acta. Metall. 34 (1986) 891-898. doi:10.1016/0001-6160(86)90062-3.

[65] M. Gazizov, S. Malopheyev, R. Kaibyshev, The effect of second-phase particles on grain refinement during equal-channel angular pressing in an Al – Cu – Mg – Ag alloy, J. Mater. Sci. 50 (2015) 990–1005. doi:10.1007/s10853-014-8659-4.

[66] P.M. Hazzledine, Grain-boundary pinning in 2-phase materials, Czech.J. Phys. 38 (1988) 431-443. doi: 10.1007/BF01605420.

Figure captions

Fig. 1. Illustration of the heat treatment and processing sequence of the Al-Zn-Mg alloy.

Fig. 2. HAADF- STEM micrographs of the Al-Zn-Mg alloy in (a,d) the as-received condition and after ECAP processing for (b,e) 4 and (c,f) 8 passes; (d), (e) and (f) are selected areas at higher magnifications in (a), (b) and (c), respectively.

Fig. 3. EDX maps of the Al-Zn-Mg alloy after ECAP for 4 passes showing an E phase along a grain boundary containing fine $MgZn_2$ precipitates.

Fig. 4. TEM micrographs of Al-Zn-Mg alloy in (a) the as-received condition and after ECAP processing for (b) 4 and (c) 8 passes.

Fig. 5. HAADF-STEM images along <100> $_{Al}$ zone axis showing second phase particles after ECAP processing for 4 passes and subsequent annealing for 20 h at (a) 393 and (b) 473 K and after 8 ECAP passes followed by annealing for 20 h at (c) 393 and (d) 473 K.

Fig.6. BF TEM along <110> $_{Al}$ after ECAP processing for 4 passes and subsequent annealing for 20 h at (a) 393 and (b) 473 K and after 8 ECAP passes followed by annealing for 20 h at (c) 393 and (d) 473 K.

Fig. 7. EDX map showing an irregular precipitate with two-η phases along a grain boundary of the Al-Zn-Mg alloy processed by 8 passes of ECAP and further heat treated at 473 K for 20 h.

Fig. 8. Zn wt% concentration in T ($Al_{18}Mg_3Cr_2$) precipitates of the Al-Zn-Mg alloy processed by (a) 4 and (b) 8 passes of ECAP and further heat treated at 393 and 473 K for 20 h and Zn wt% concentration in E ($Al_{20}Cu_2Mn_3$) phases of the Al-Zn-Mg alloy processed by (c) 4 and (d) 8 passes of ECAP and further heat treated at 393 and 473 K for 20 h.

Fig. 9. TEM images showing precipitates in the Al-Zn-Mg alloy after ECAP processing for (a) 4 and (b) 8 passes followed by heat treatment at 473 K for 20 h.

Fig. 10. HRTEM images of the Al-Zn-Mg alloy after ECAP processing for 4 passes and heat treatment at 393 K for 20 h showing (a) overlapped T and E phases, (b) T phase containing fine η precipitates, (c) a lattice mismatch between the E and the T phases and (d) FFT pattern of the T and E phase.

Fig. 11. HRTEM images of twin planes of overlapped T and E phases in (a) and (b) higher magnification of the twin plane and FFT pattern showing the twinning planes, (c) IFFT showing dislocation pair, (d) and (e) IFFT presenting a group of dislocations surrounding the twinning planes.

Table captions

Table 1. Summary of structure information of second phases in Al-Zn-Mg alloys [36-39].

Phase	Composition	Crystal structure	Space group	Lattice parameter
η'	Zn:Mg = 1:1 to 1.5:1	Monoclinic Hexagonal	P6m2	a = 0.497 nm, c = 0.554 nm a = 0.496 nm, c = 1.402 nm
η	$MgZn_2$	hcp	P63/mmc	a = 0.516-0.522 nm , c = 0.849-0.860 nm
E	$Al_{18}Mg_3Cr_2$	fcc	$Fd\bar{3}m$	a = 1.4526 nm.
T	$Al_{20}Cu_2Mn_3$	B-centered orthorhombic structure	Bbmm	a = 2.398 nm, b = 1.254 nm, c = 0.766 nm
Al_3Zr	Al_3Zr	Tetragonal	I4/mmm	a = 4.005 nm, c = 17.285 nm

Table 2. Element contents of random selected T and E particles in the as-received and ECAP-processed Al-Zn-Mg alloy detected by EDX (in wt.%)

State	phase	Al	Mg	Mn	Cr	Cu	Zn
As-received	T	80	1	10.4	0.8	4.1	0.8
	E	84	8.2	0.8	4.5	0.05	0.78
ECAP for 4 passes	T	83.1	1.8	6.6	1.3	4.1	2.6
	E	84.3	9.7	0.3	4.2	1.3	2.2
ECAP for 8 passes	T	87	1.9	5.9	0.8	3.1	2.5
	E	86	9.5	0.4	3.9	1	1.8

Table 3 Summary of microstructural features in the as-received, ECAP-processed and post-ECAP annealed Al-Zn-Mg alloy

	As-received	ECAP , 4 passes	ECAP, 8 passes	ECAP, 4 passes + Annealing, 393 K×20 h	ECAP, 4 passes + Annealing, 473 K×20 h	ECAP, 8 passes + Annealing, 393 K×20 h	ECAP, 8 passes + Annealing, 473 K×20 h
Grain size	1.3 μm	200 nm	190 nm	230 nm	240 nm	210 nm	230 nm
Precipitates type (size/nm)	G.P. (5) η' (120) T & E (180)	G.P.,η', η, T, E (~60)	η', η, T, E (~65)	η', η (~13.5) T, E (~82)	η',η (~21) T, E (~114)	η', η (~14) T , E (~76)	η' , η (~11) η, T, E (Length:~140)

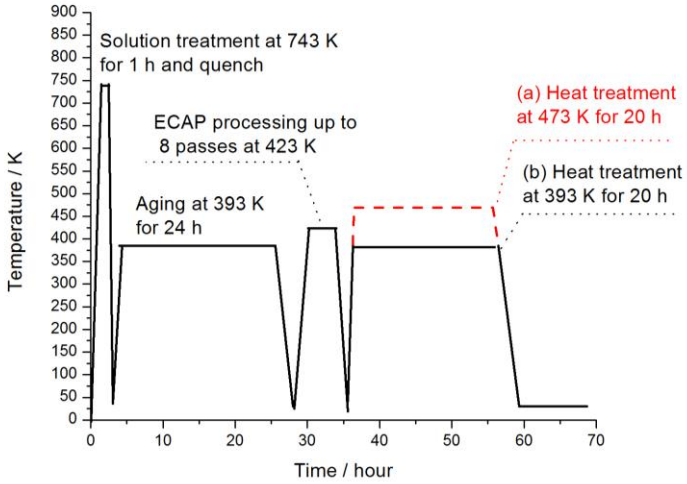

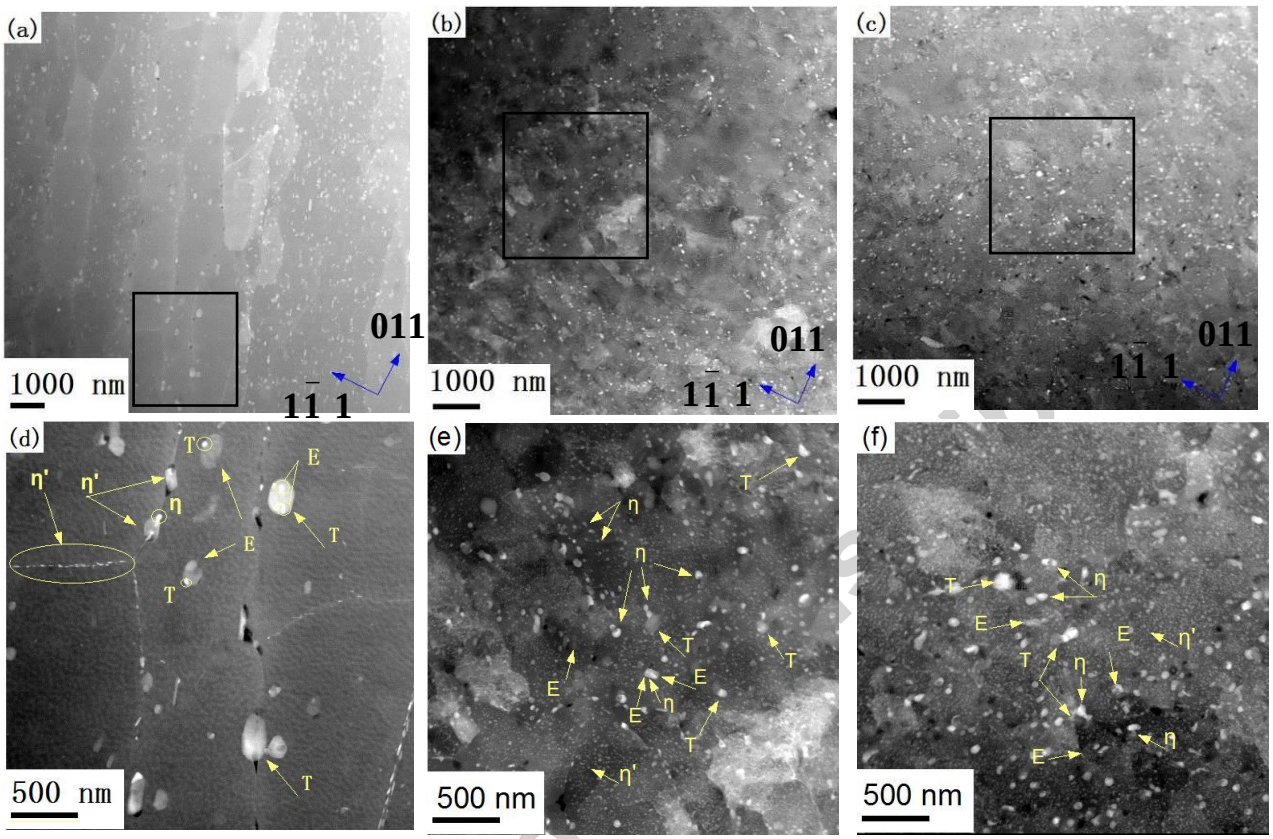

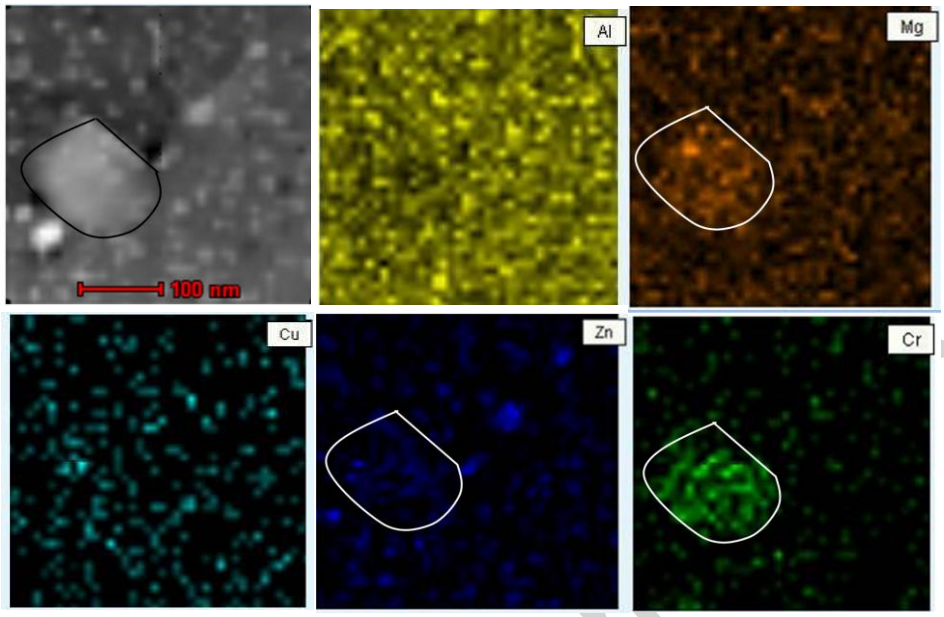
100 nm
Al
Mg
Cu
Zn
Cr

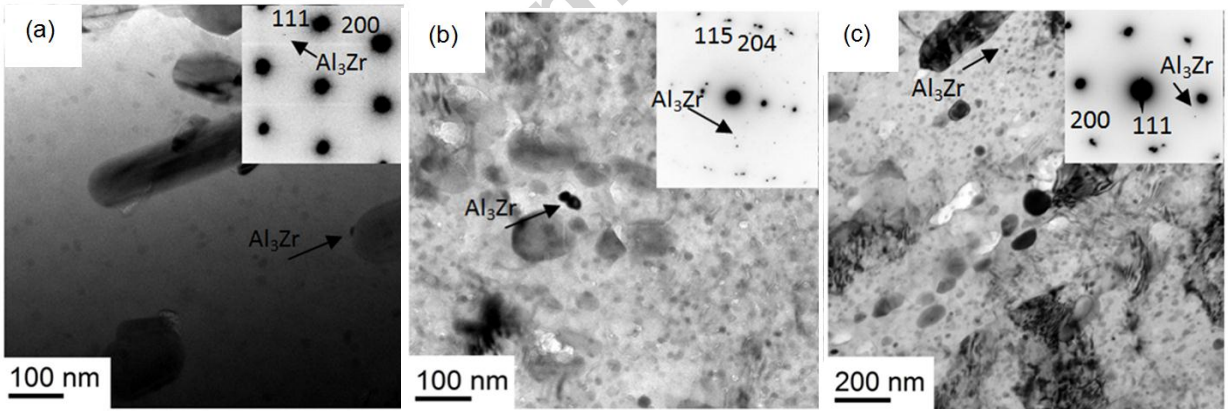
(a)
111
200
Al3Zr
Al3Zr
100 nm
(b)
115
204
Al3Zr
Al3Zr
100 nm
(c)
Al3Zr
Al3Zr
200
111
200 nm

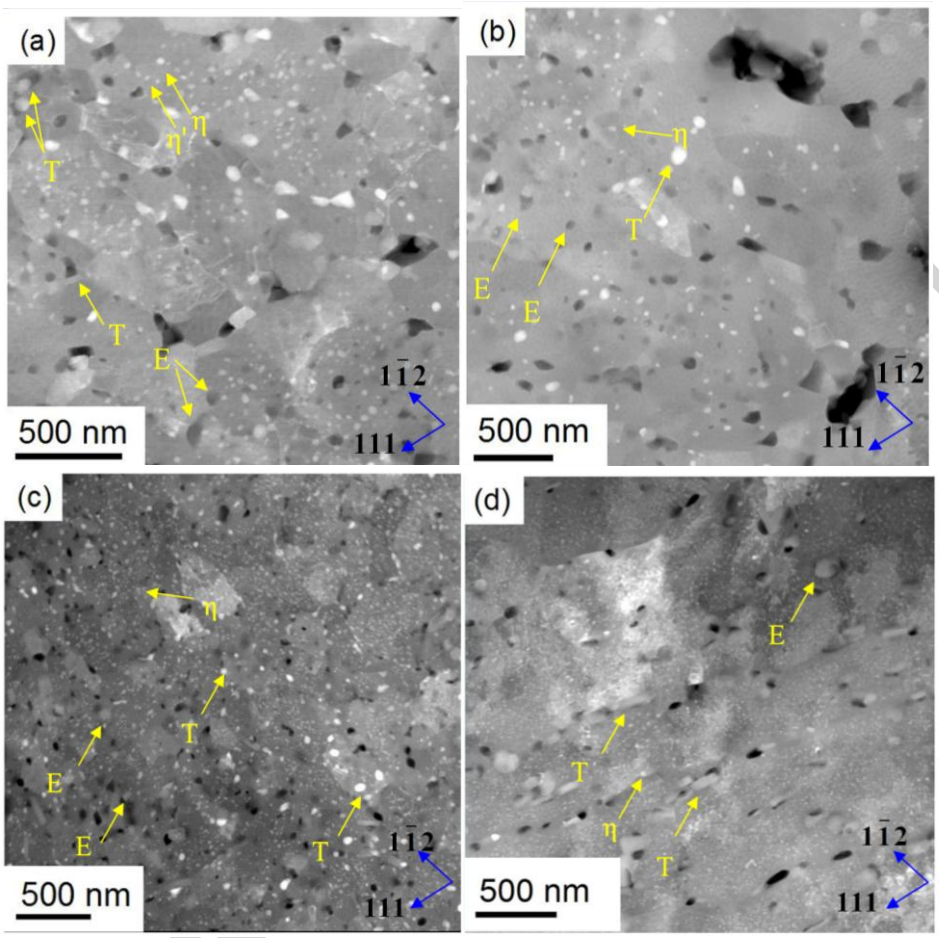
(a)
η
η'
T
T
E
500 nm
1$\bar{1}$2
111
(b)
η
T
E
E
500 nm
1$\bar{1}$2
111
(c)
η
T
E
E
T
500 nm
1$\bar{1}$2
111
(d)
E
T
η
T
500 nm
1$\bar{1}$2
111

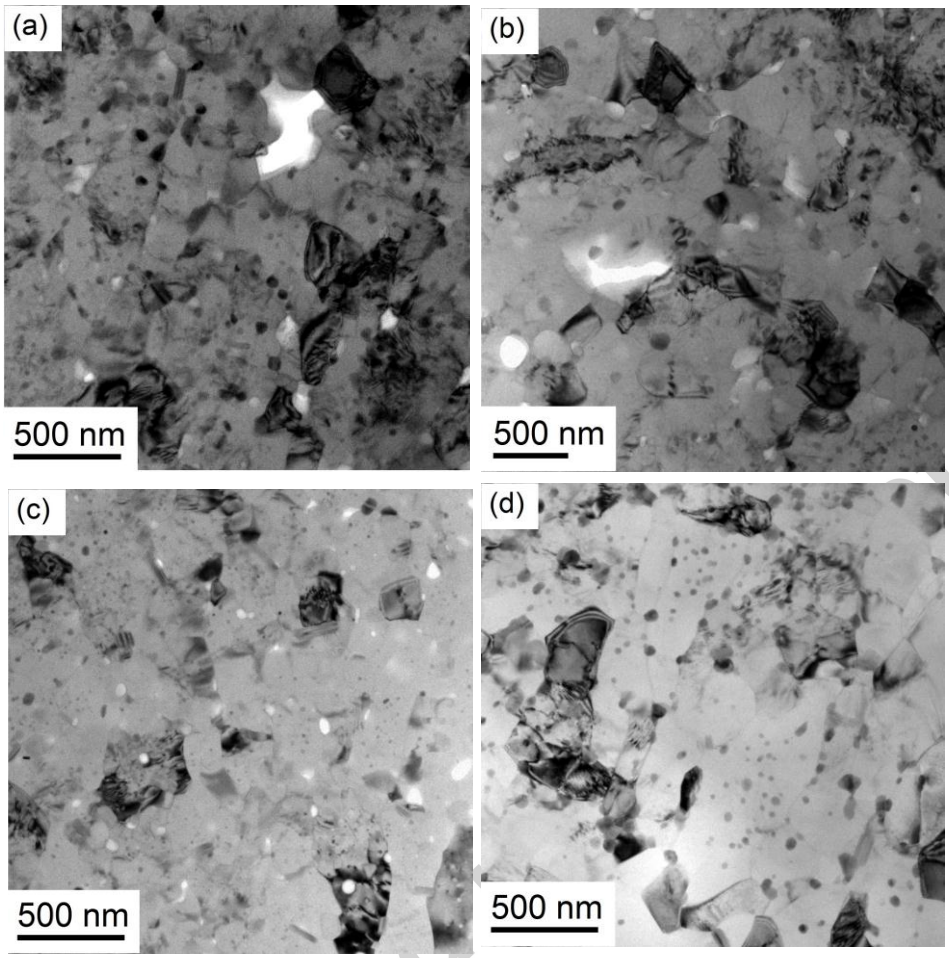
(a)
500 nm
(b)
500 nm
(c)
500 nm
(d)
500 nm

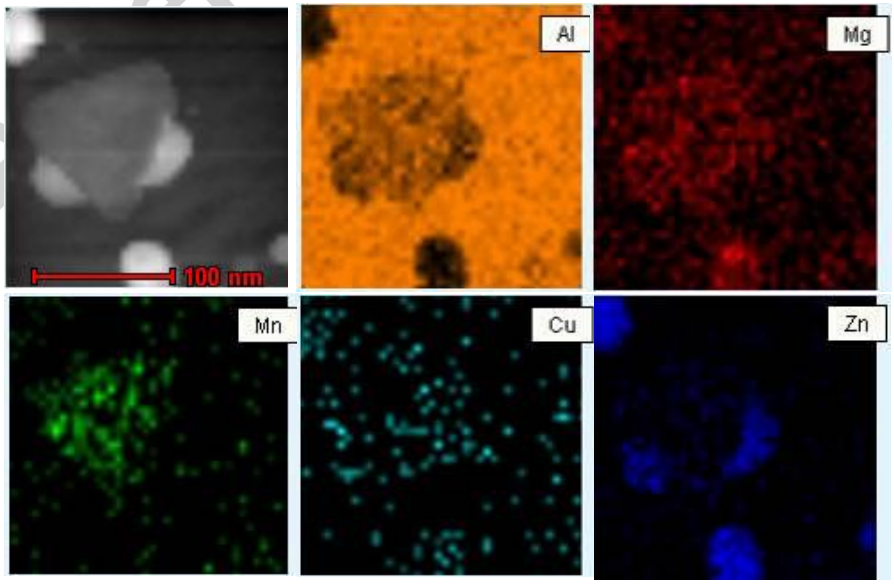
100 nm
Al
Mg
Mn
Cu
Zn

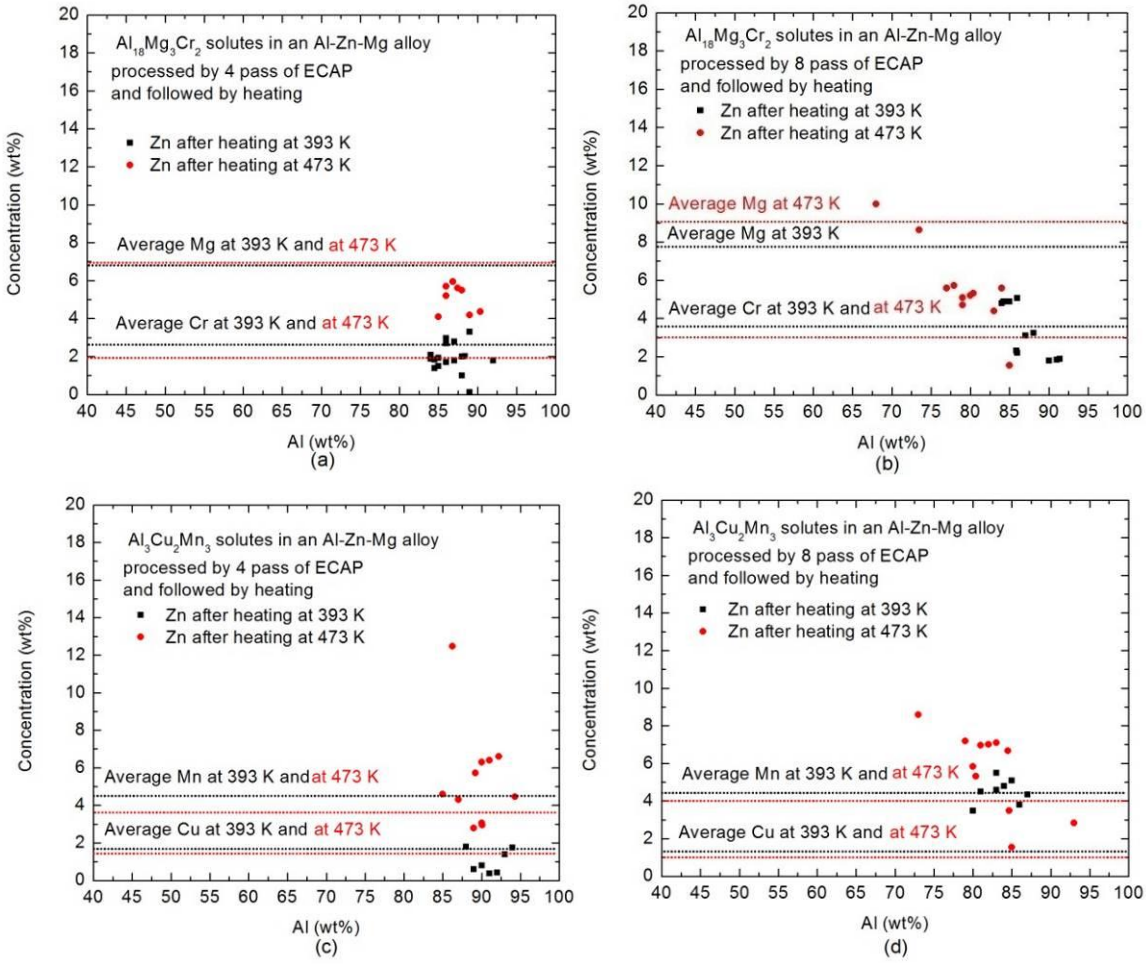
$Al_{18}Mg_3Cr_2$ solutes in an Al-Zn-Mg alloy
processed by 4 pass of ECAP
and followed by heating
Zn after heating at 393 K
Zn after heating at 473 K
Average Mg at 393 K and at 473 K
Average Cr at 393 K and at 473 K
Concentration (wt%)
Al (wt%)
(a)
$Al_{18}Mg_3Cr_2$ solutes in an Al-Zn-Mg alloy
processed by 8 pass of ECAP
and followed by heating
Zn after heating at 393 K
Zn after heating at 473 K
Average Mg at 473 K
Average Mg at 393 K
Average Cr at 393 K and at 473 K
Concentration (wt%)
Al (wt%)
(b)
$Al_3Cu_2Mn_3$ solutes in an Al-Zn-Mg alloy
processed by 4 pass of ECAP
and followed by heating
Zn after heating at 393 K
Zn after heating at 473 K
Average Mn at 393 K and at 473 K
Average Cu at 393 K and at 473 K
Concentration (wt%)
Al (wt%)
(c)
$Al_3Cu_2Mn_3$ solutes in an Al-Zn-Mg alloy
processed by 8 pass of ECAP
and followed by heating
Zn after heating at 393 K
Zn after heating at 473 K
Average Mn at 393 K and at 473 K
Average Cu at 393 K and at 473 K
Concentration (wt%)
Al (wt%)
(d)

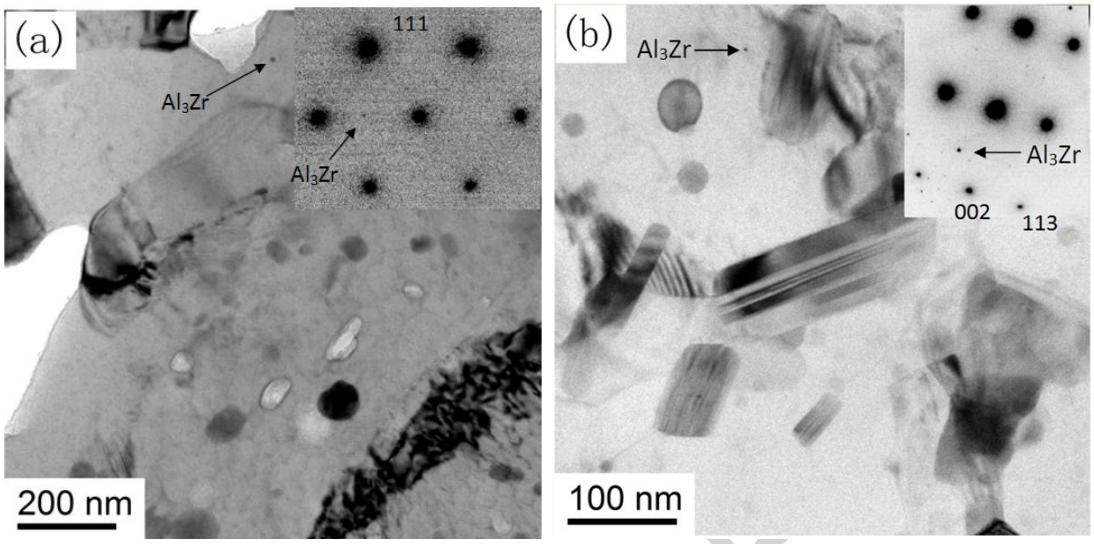

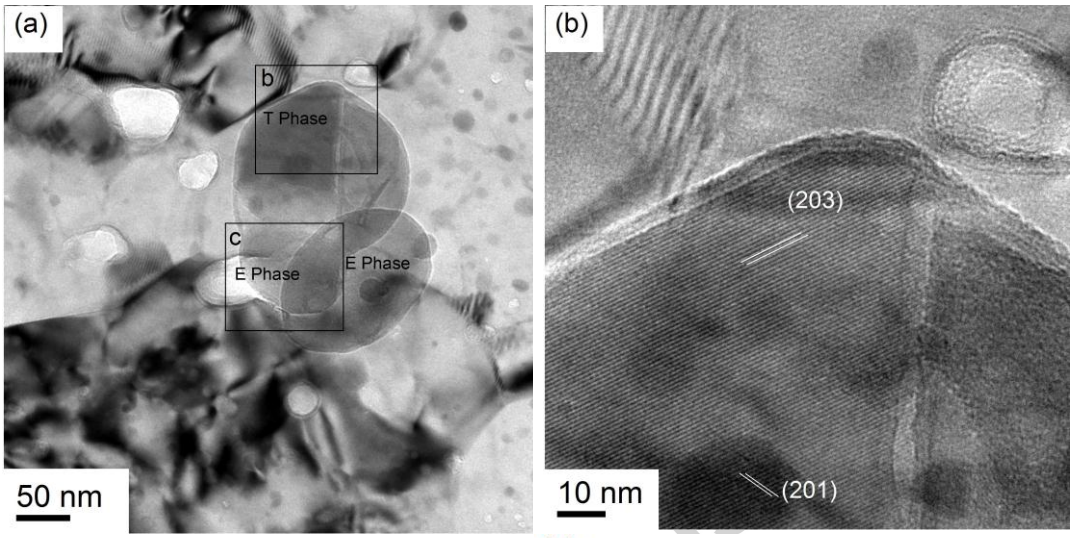
(a)
b
T Phase
c
E Phase
E Phase
50 nm
(b)
(203)
(201)
10 nm

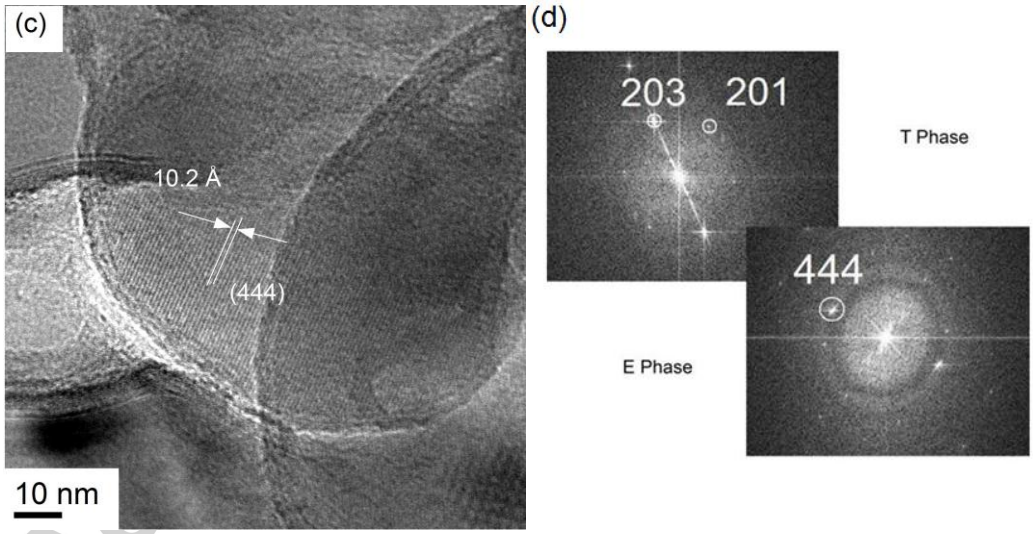
(c)
10.2 Å
(444)
10 nm
(d)
203 201
T Phase
444
E Phase